Atomic diffraction from nanostructured optical potentials

G. Lévêque, C. Meier, R. Mathevet, C. Robilliard, and J. Weiner
Laboratoire de Collisions, Agrégats et Réactivité, UMR 5589 du CNRS et l'Université Paul Sabatier, Institut de Recherche sur les Systèmes Atomiques et Moléculaires Complexes, Université Paul Sabatier, 31062 Toulouse Cedex 4, France

C. Girard
Centre d'Elaboration de Matériaux et d'Etudes Structurales, 29, rue Jeanne Marvig, Boîte Postale 4347, 31055 Toulouse Cedex 4, France

J. C. Weeber
Laboratoire de Physique de l'Université de Bourgogne, 9 Avenue A. Savary, F-21078 Dijon, France
(Received 9 July 2001; revised manuscript received 11 December 2001; published 9 May 2002)

We develop a versatile theoretical approach to the study of ultracold atom diffractive scattering from light-field gratings by combining calculations of the optical near field generated by evanescent waves close to the surface of periodic nanostructured arrays with atom wavepacket propagation techniques. Nanometric one dimensional (1D) and 2D arrays with subwavelength periodicity deposited on a transparent surface and optically coupled to an evanescent wave source exhibit intensity and polarization gradients on the length scale of the object and can produce strong near-field periodic modulation in the optical potential above the structure. As a specific and experimentally practical example we calculate the diffraction of cold Cs atoms dropped onto a periodic optical potential crafted from a 2D nanostructure array. For an ''out-of-plane'' configuration we calculate a wide diffraction angle ($\simeq 2°$) and about 60% of the initial atom flux in diffraction orders ± 1, an encouraging result for future experiments.

DOI: 10.1103/PhysRevA.65.053615 PACS number(s): 03.75.Be, 32.80.Lg

I. INTRODUCTION

The prospect of manipulating neutral atoms and molecules by light forces acting at nanometer scale lengths offers fascinating but experimentally challenging possibilities in many areas of atomic physics. Atom optics [1], atom nanolithography [2,3], and atom interferometry [1] are prime examples. The use of high-refractive-index dielectric or metallic nanometric objects to produce subwavelength localized light-field distributions [4–6] raises the possibility of ''integrated atom optics'' in which atoms or molecules can be confined, guided, or diffracted above nanostructured surfaces fabricated to a designed shape [7–9]. Tailoring optical potentials for atom control, and possibly Bose-Einstein condensates, is analogous to the use of micromagnetic fields for a similar purpose [10–18]. Atom diffraction from a transmission optical grating provided one of the early examples of light-field atom manipulation [19]. A proposal for [20] and realization of [21] a reflection light-field grating quickly followed. These early developments stimulated many subsequent experimental and theoretical studies, and a pertinent review has recently appeared [22]. Until now reflection gratings for matter waves have been implemented by the formation of one-dimensional evanescent standing waves produced by counterpropagating laser beams undergoing total internal reflection through a glass prism.

The approach we present here contrasts markedly with this earlier work on standing waves of sinusoidal form. We study diffractive scattering of cold atoms from an evanescent field, spatially modulated by an array of nanometric objects with high index of refraction and subwavelength periodicity deposited on a glass surface [23,24]. These evanescent fields and their interaction with atoms will exhibit several important features. First, rather than a pure sinusoidal evanescent standing wave, nanostructured periodic corrugation generates fields containing higher-order harmonics and an intricate polarization distribution. Second, spatial gradients of field intensity and polarization at length scales well below the diffraction limit interact with the external and internal atomic degrees of freedom in ways that strongly depend on the geometry and material of the nanostructures employed. Third, the intensity and polarization map above the nanostructure array also depends strongly on the intensity and polarization of the exciting light source.

Since the cold-atom de Broglie wavelength is not much smaller than the characteristic scale length of the optical field, an accurate description of atomic motion calls for a quantum treatment of external as well as internal degrees of freedom. In order to analyze the dynamics of cold atoms scattering off periodic optical potentials we need to combine two well-developed numerical techniques: calculation of the optical near field and atom wave packet propagation. The situation we consider is shown in Fig. 1. First, we calculate the three-dimensional electric field and polarization distribution in the near field surrounding the nanostructures. At frequency detunings far from resonance, where absorption is negligible, this information is used to construct a conservative potential for a full three-dimensional treatment of the center-of-mass motion of the atom, including ground internal states. Using the light-field information above the nanostructures, we calculate the three-dimensional atom-field interaction potential [22,25,26]. Since the field polarization will

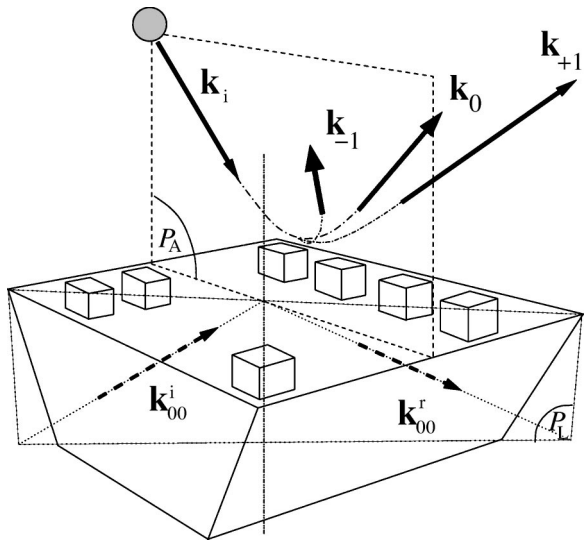

FIG. 1. Schematic diagram of cold-atom diffraction off an optical potential. The atom impinges on the periodic potential with incident wave vector $\mathbf{k}_i$ and diffracts into orders $\mathbf{k}_{\pm 1}, \mathbf{k}_0$. The periodic optical near field above the nanostructured array is generated by light with incident wave vector $\mathbf{k}^i_{00}$, totally internally reflected into $\mathbf{k}^r_{00}$. The nanostructures are cubes of a high-refractive-index material with subwavelength dimensions and periodicity (see text for model details). Note that the incident plane of the light P_L is along the diagonal of the cubes while the incident plane of the atoms P_A is shifted 45° and parallel to the cube edges. Note also that the diffracted orders $\mathbf{k}_{\pm 1}$ are "out of plane" with respect to the plane of incidence of the atoms.

vary significantly over the length scale of the nanostructures [27], and since various field polarizations may lead to population transfer among atomic internal states [22], we include the internal Zeeman states of a $^2S_{1/2}$ atomic ground level in the calculation of the atom–optical field scattering. Second, we apply a time-dependent wave packet method to describe the scattering problem of cold atoms diffracting from an optical grating with subwavelength periodicity. Inclusion of the ground-level internal states leads to a three-dimensional, coupled channel problem that we solve with wave packet propagation techniques already successfully applied to atom or molecule surface scattering and quantum molecular dynamics in several degrees of freedom [28–38]. After the wave packet representing the atom reflects and diffracts from the optical potential, it is projected onto final scattering states to yield the desired diffraction probabilities [35].

In this paper we emphasize general principles and seek to establish a methodology without restriction to any specific experimental setup. In fact, the numerical solution of Maxwell's equations in the near field and Schrödinger's equation for the atomic motion can easily be adapted to explore atom manipulation in subwavelength optical light fields of arbitrary geometry. However to illustrate this methodology we present calculations obtained with realistic parameters corresponding to an experiment using a flux of cold $^2S_{1/2}$ atoms incident at about 40° from the normal and scattering off a two-dimensional optical grating with subwavelength period. The results of our calculation yields out-of-plane diffraction into a few orders, with markedly large diffraction angles. The results are encouraging for planned experiments.

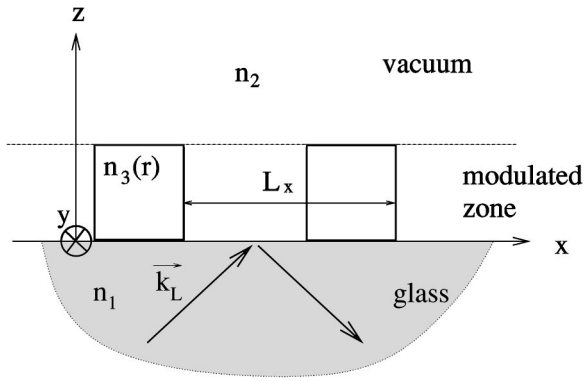

FIG. 2. Schematic representation of the three optical regions to which the differential method of gratings is applied.

The rest of the paper is organized as follows. Section II gives details of the calculation of the scattering probabilities. The subwavelength light-field calculations are reported elsewhere [27], so only the essential steps are summarized here. In Sec. III we present a model configuration and in Sec. IV we show the numerical results for illustration.

II. THEORY

A. The optical near field

The evanescent wave field created by the totally internally reflected laser beam is strongly modified by the periodic nanostructures on the glass substrate surface. The calculation of this intricate electric vector field above the nanostructures can be carried out using several methods that solve Maxwell's equations in these nontrivial geometries. These methods are well established in the field of scanning near-field optical microscopy (SNOM) [4,6]. Among the most widely used are the finite-differences scheme [39], the differential theory of gratings (DTG) ([40–42]), and the Green's function method [4]. This latter approach is well adapted to study single, finite-size nano-objects, and has been used extensively to study a wide range of nanostructures [43,44]. However, in the case of periodic surface structures, it becomes inefficient, since it does not explicitly take the periodicity into account. In such cases, the DTG method is more appropriate, because it solves Maxwell's equations by means of a Fourier expansion of each field component.

To be more specific, we define $\mathbf{r}=(x,y,z)$ with z taken as the direction perpendicular to the surface. For convenience, we define a vector $\mathbf{l}=(x,y)$ in the plane of the substrate surface. We will denote the electric field by 1 in the glass half space and by 2 in the vacuum half space, n_1 being the glass index and n_2 the vacuum index. The two-dimensional periodicity of the nanostructures defines a unit cell of length L_x and L_y along the x and y directions, respectively. The direction of the incoming laser is given by (k_L^x, k_L^y, k_L^z), with $k_L = n_1 2\pi/\lambda_0 = n_1 k_0$, and λ_0 being the laser wavelength in vacuum.

In the DTG method, an index-modulated zone, labeled 3 and characterized by $n_3(\mathbf{r})$, the high index material, is intro-

duced at the vacuum/glass substrate interface, as shown in Fig. 2. In the glass and vacuum half spaces, n_1, n_2, the electromagnetic field obeys Helmholtz's equation

$$\Delta \mathbf{E}^{(l)}(\mathbf{r}) + n_l^2 k_0^2 \mathbf{E}^{(l)}(\mathbf{r}) = 0, \quad l = 1,2$$

In the modulated zone, this equation is not valid because of the discontinuities of $n_3(\mathbf{r})$. In this region, we integrate directly Faraday's and Ampere's equations,

$$\nabla \times \mathbf{E}^{(3)} = i\omega \mathbf{B}^{(3)},$$

$$\nabla \times \mathbf{B}^{(3)} = -i\omega \epsilon_0 \mu_0 n_3^2 \mathbf{E}^{(3)}.$$

Since the system is periodic along x and y we can expand the dielectric constant (i.e., n_3^2) in the modulated zone,

$$n_3^2(\mathbf{r}) = \sum_{n,m} \alpha_{mn} \exp\left[2i\pi\left(\frac{nx}{L_x} + \frac{my}{L_y}\right)\right],$$

where α_{mn} are the Fourier coefficients of n_3^2. It is clear that electric and magnetic fields *outside* the modulated zone will also be periodic and thus conveniently written,

$$\mathbf{E}^{(l)}(\mathbf{r}) = \sum_{m,n=-\infty}^{\infty} \mathbf{E}_{mn}^{(l)} e^{i\gamma_{mn}^l z} e^{i\mathbf{k}_{mn}^{\parallel}\cdot\mathbf{l}}, \tag{1}$$

$$\mathbf{B}^{(l)}(\mathbf{r}) = \sum_{m,n=-\infty}^{\infty} \mathbf{B}_{mn}^{(l)} e^{i\gamma_{mn}^l z} e^{i\mathbf{k}_{mn}^{\parallel}\cdot\mathbf{l}}; \quad l = 1,2. \tag{2}$$

In this expression, $\mathbf{k}_{mn}^{\parallel}$ denote the x,y components of the wave vector of the field diffracted in the (m,n) order, and is given by $\mathbf{k}_{mn}^{\parallel} = (k_L^x + 2\pi m/L_x, k_L^y + 2\pi n/L_y)$. The z component of the wave vector γ_{mn} obeys the dispersion equation

$$(\mathbf{k}_{mn}^{\parallel})^2 + (\gamma_{mn}^l)^2 = n_l^2[(k_0^x)^2 + (k_0^y)^2 + (k_0^z)^2] \tag{3}$$

for which we have two solutions, corresponding to ''rising'' and ''descending'' waves. The rising zero order in the glass substrate corresponds to the incident laser field. Then, if we know the Fourier components $\mathbf{E}_{mn}$ and $\mathbf{B}_{mn}$ of the electric and magnetic field in a plane just above the nano-objects, the field distribution anywhere above the structures is determined by Eqs. (1) and (2). From Eq. (3), it may be seen that the coefficient γ_{mn} is either real or purely imaginary. The real values of γ_{mn} correspond to radiative harmonics while imaginary values introduce evanescent components.

The six components of the electromagnetic field $\mathbf{E}^{(l)}(\mathbf{r}), \mathbf{B}^{(l)}(\mathbf{r})$ are then deduced from two independent parameters, usually named *the principal components*, which in the present case are chosen to be the y components $E^{(l)y}(\mathbf{r})$ and $B^{(l)y}(\mathbf{r})$. In order to calculate the principal Fourier components of the electric field just above the nanostructures, we have to solve a system of linear differential equations for $E^{(3)x,y}(\mathbf{r})$ and $B^{(3)x,y}(\mathbf{r})$ in the region of space where the index is modulated by the nanostructures. This system mixes all the Fourier orders of the electric and the magnetic field through the product between n_3^2 and $\mathbf{E}^{(3)}(\mathbf{r})$ appearing in Ampere's equation. Then, for numerical applications, the Fourier expansion converges at some sufficiently large value N. The orders n and m will both vary from $-N$ to $+N$. We solve this system using standard boundary conditions for this problem, i.e., we assume there is no field arriving from infinity in the vacuum, and the only Fourier components of the incident field in the glass substrate are those of zero order. Finally, we can express the Fourier components $E_{mn}^{(2)y}$ and $B_{mn}^{(2)y}$ in a horizontal plane just above the nano-objects as a linear combination of the y components of the incident fields, E_i, B_i, which define the polarization state of the incoming laser,

$$E_{mn}^{(2)y} = \mathcal{T}_{mn}^{EE} E_i^{(1)y} + \mathcal{T}_{mn}^{EB} B_i^{(1)y}, \tag{4}$$

$$B_{mn}^{(2)y} = \mathcal{T}_{mn}^{BE} E_i^{(1)y} + \mathcal{T}_{mn}^{BB} B_i^{(1)y}. \tag{5}$$

These transmission coefficients, $\mathcal{T}_{mn}^{EE}$, $\mathcal{T}_{mn}^{EB}$, $\mathcal{T}_{mn}^{BE}$, and $\mathcal{T}_{mn}^{BB}$ depend only on the geometry of the sample, the frequency, and the angle of incidence of the illuminating laser. The setup for the field calculation is shown in Fig. 2. A more detailed description of this calculation can be found in Refs. [40,42]. With the optical field mapping in hand we turn our attention to atom scattering in the presence of these fields.

B. Calculation of atom-surface scattering

In the limit of low saturation and a blue detuning δ that is large compared to the Doppler shift and natural linewidth, the atom-field interaction can be treated within the framework of coherent atomic motion where spontaneous emission is neglected [22,25,26]. We will consider an atom transition dipole, typical of the first alkali $^2S_{1/2} \rightarrow {}^2P_{3/2}$ transition, neglecting hyperfine structure, but including the two-component angular momentum degeneracy of the ground state. The excited level can be eliminated adiabatically, which results in atomic motion that is described by a two-component, three-dimensional wave packet that evolves on the ground-state manifold of the Zeeman sublevels [22,25,26],

$$i\hbar \frac{\partial \Psi_{m_j}(\mathbf{r})}{\partial t} = T_{\mathbf{r}} \Psi_{m_j} + \sum_{m_j' = \pm 1/2} V_{m_j m_j'}(\mathbf{r}) \Psi_{m_j'}(\mathbf{r}). \tag{6}$$

In this expression, the operator of the kinetic energy is simply given by

$$T_{\mathbf{r}} = -\frac{\hbar^2}{2M} \nabla_{\mathbf{r}}^2, \tag{7}$$

with M being the mass of the atom. The potential within the low saturation limit can be written as [22,25,26]

$$V_{m_j m_j'}(\mathbf{r}) = \frac{d^2}{\hbar \delta} \sum_{q,q',m_e} E_q^*(\mathbf{r}) E_{q'}(\mathbf{r}) (j_g, m_j; 1, q | j_e, m_e) \times (j_e, m_e | j_g, m_j'; 1, q'). \tag{8}$$

In this expression the terms in parentheses are Clebsch-Gordan coefficients with j_g and j_e being the total angular momentum of the ground and excited states, respectively.

The reduced dipole moment is denoted by d and the field enters through its spherical components $E_q(\mathbf{r})$, $q=0,\pm 1$. This expression forms the basis of numerous studies of atomic diffraction from standing evanescent waves as has been used by many authors [8,22,25,26,45]. In general, the polarization state of the electric field above the nanostructured objects is a very complicated function of space. Hence, according to Eqs. (6) and (8), transitions between the different Zeeman sublevels can occur during the interaction of the atom with the light fields. As a consequence, we performed the calculation including coupling of the two ground state levels.

One way of proceeding is to expand the wave function into plane waves parallel to the surface, which results in a set of coupled diffraction channels for the direction perpendicular to the surface [22]. Diffraction then occurs as transitions between these diffractive states, the probabilities of which can be calculated by a semiclassical treatment within the Landau-Zener theory [22], or by numerical wave packet propagation [45]. This treatment corresponds to the well-known close-coupling wave packet method used in standard atom or molecule surface scattering [46]. However, with increasing diffraction orders one may need to take a large number of diffractive states into account, together with all the coupling matrix elements among them. In fact, it is only recently that modern and very efficient numerical wave packet propagation techniques have permitted the calculation of diffractive scattering by solving Eq. (6) directly on grids in real space [28,36,37]. Briefly, one simulates the collisional process by a wave packet propagation from the initial state to the final interaction-free zone, where it is projected onto any desired observable, which in our case is the total population in the different diffraction channels. To achieve a good energy resolution, one needs to construct an initial wave packet that is sufficiently large such that its energy width is negligible. From a numerical point of view, this is very disadvantageous, since it requires a large grid in the direction perpendicular to the surface. Therefore, we used a method proposed by Mowrey and Kouri [46], who started with a spatially narrow wave packet that comprised a wide range of energies, and extracted energetically resolved results by projecting onto asymptotic states of well-defined energy, $\mathcal{E}$.

The initial state of the atom is taken to be a specific Zeeman sublevel $m_j=-1/2$ of the ground state manifold with center-of-mass motion described by the box-normalized wave function

$$\Psi^i_{m_j}(\mathbf{r})=(2\pi\xi^2L_x^2L_y^2)^{-1/4}\times\exp[-(z-z_0)^2/4\xi^2+ik_i^z z+i\mathbf{k}_i\cdot\mathbf{l}], \tag{9}$$

with the initial transverse momentum $\mathbf{k}_i=(k_i^x,k_i^y)$ and the initial momentum in z direction described by a Gaussian distribution centered around k_i^z. The propagation of this three-dimensional wave packet is performed on the coupled surfaces defined by Eqs. (6) and (8) until the final scattered wave function $\Psi^f_{m_j}(\mathbf{r})$ is entirely in the asymptotic region.

The (unnormalized) modulus square of the transition amplitudes is given by projection of the final wave packet onto diffractive states [46],

$$|b^{mn}_{m_j}(\mathcal{E})|^2=\frac{1}{k^z_{mn}}\left|\int d\mathbf{r}\exp\{-i[k^z_{mn}z+(\mathbf{k}_i+\mathbf{G}_{mn})\cdot\mathbf{l}]\}\times\Psi^f_{m_j}(\mathbf{r})\right|^2, \tag{10}$$

where $\mathbf{G}_{mn}=(2\pi m/L_x,2\pi n/L_y)$ denotes the reciprocal-lattice vector and k^z_{mn} is determined by energy conservation,

$$k^z_{mn}=\sqrt{2M\mathcal{E}-(\mathbf{k}_i+\mathbf{G}_{mn})^2}. \tag{11}$$

The probability to diffract into a specific order (m,n) as a function of total collision energy is then given by [37,46]

$$P(m,n)=\left(\sum_{m_j=\pm 1/2}|b^{mn}_{m_j}(\mathcal{E})|^2\right)\Big/\left(\sum_{m_j=\pm 1/2}\sum_{mn}|b^{mn}_{m_j}(\mathcal{E})|^2\right). \tag{12}$$

This quantity will be calculated for a selected set of parameters and discussed in the following section. For the three-dimensional, two-component wave packet propagation we used the fast Fourier transform (FFT)-split-operator scheme, which in the field of quantum molecular dynamics or molecule-surface collisions has proven to be a fast, stable, and efficient method to perform this task [47]. Briefly, in this method the total quantum mechanical short-time propagator is approximated by

$$\begin{aligned}\exp\left[-i\frac{\Delta t}{\hbar}\begin{pmatrix}T_{\mathbf{r}}+V_{1/2,1/2}(\mathbf{r}) & V_{1/2,-1/2}(\mathbf{r})\\ V_{-1/2,1/2}(\mathbf{r}) & T_{\mathbf{r}}+V_{-1/2,-1/2}(\mathbf{r})\end{pmatrix}\right]&\\ \approx\exp\left[-i\frac{\Delta t}{2\hbar}\begin{pmatrix}T_{\mathbf{r}} & 0\\ 0 & T_{\mathbf{r}}\end{pmatrix}\right]&\\ \times\exp\left[-i\frac{\Delta t}{\hbar}\begin{pmatrix}V_{1/2,1/2}(\mathbf{r}) & V_{1/2,-1/2}(\mathbf{r})\\ V_{-1/2,1/2}(\mathbf{r}) & V_{-1/2,-1/2}(\mathbf{r})\end{pmatrix}\right]&\\ \times\exp\left[-i\frac{\Delta t}{2\hbar}\begin{pmatrix}T_{\mathbf{r}} & 0\\ 0 & T_{\mathbf{r}}\end{pmatrix}\right].&\end{aligned} \tag{13}$$

This form of symmetric splitting is correct through second order; it is unitary by construction and thus ensures numerical stability [47,48]. The operator acts on the two-component wave function to perform a short-time propagation from time t to $t+\Delta t$. The action of the kinetic operator is calculated in Fourier space, where it is a simple multiplication with a phase factor, and so every time step the two components of the wave functions need to be Fourier transformed, which can be done very efficiently with three-dimensional FFT algorithms. With this technique, the initial wave packet Eq. (9) is propagated until it is entirely in the asymptotic region. The distance from which the wave packet can be considered effectively free has to be checked carefully since it depends on many parameters. This is especially important in the field of cold collisions where low energies are considered.

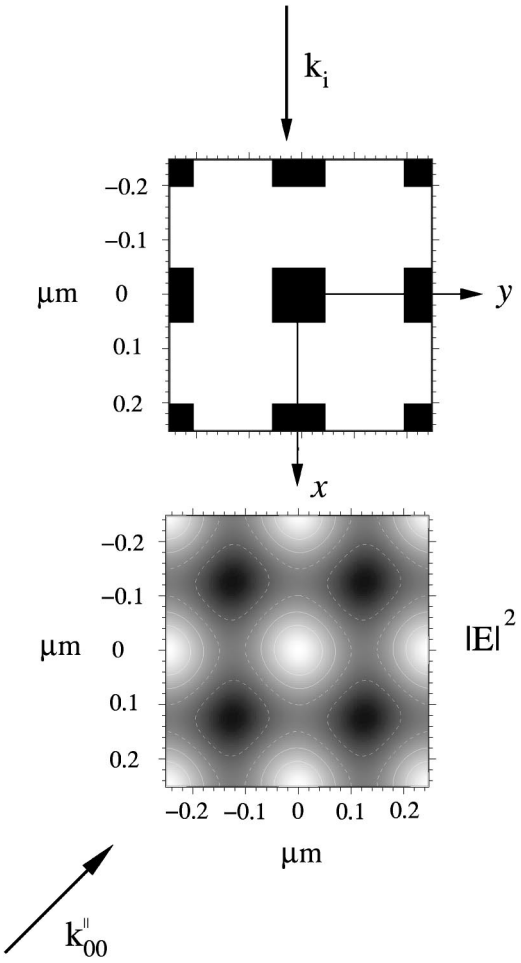

FIG. 3. Top panel, schematic view of the 100 nm TiO_2 cubes deposited on a silica surface. Bottom panel, light-field intensity distribution 125 nm above the nanostructures (the arrow $\mathbf{k}_{00}^{\parallel}$ indicates the plane of the incident laser of mode TM and $\mathbf{k}_i$ the plane of incidence of the atoms). The contour lines correspond to (in units of $|E_i|^2$) 0.397, 0.412 (dashed lines) and 0.427, 0.442 (solid lines).

Even though not applied in the current approach, we note that the numerical effort can still be reduced by an adiabatic correction of the initial state [36,37,49], analyzing the flux out of the scattering region instead of projecting onto final diffractive states [49,50] or using a filter-diagonalization scheme [51].

III. NUMERICAL IMPLEMENTATION

A. Model configuration

We model a typical experimental setup with a regular square lattice of TiO_2 cubes (100 nm on a side, index of refraction $n=2.1$) deposited onto a flat silica surface (index of refraction $n=1.5$) at a center-to-center distance of 250 nm (Figs. 1, 3, and 4). These structures are illuminated by an evanescent light field created by an incoming laser with a vacuum wavelength of 850 nm, intensity of 80 W/cm^2, and subject to total internal reflection. The plane of incidence of the laser beam (denoted $\mathbf{k}_{00}^{\parallel}$ in Figs. 1 and 3) is chosen to be diagonal with respect to the rectangular nanostructured pattern, and its polarization is taken to be within the plane of incidence (TM polarization). The angle of incidence with respect to the surface normal was chosen to be 60°. Under these conditions, the flat surface without the nanostructures would give rise to an evanescent wave with a decay length γ_{00} of about 170 nm, and the atoms would not approach closer than about 200 nm to the surface. Hence the influence of the attractive van der Waals atom-surface potential can be neglected. For different parameters, however, it might become important [52], and can easily be included in Eqs. (6) and (8). The Fourier decomposition Eq. (1) required $N=10$ terms for convergence.

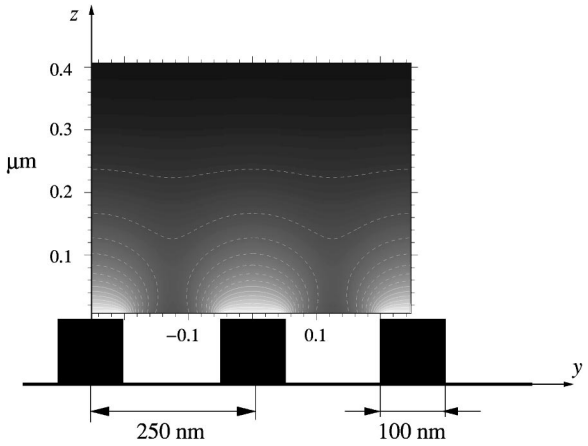

FIG. 4. Light-field intensity distribution in the y,z plane together with a schematic view of the TiO_2 nanostructures deposited on the silica surface. The contour lines correspond to (in units of $|E_i|^2$) 0.080, 0.135, 0.189, 0.241, 0.293, 0.346, 0.400 (dashed lines, from top to bottom).

B. Diffractive scattering

We have chosen a model atom with ground state $^2S_{1/2}$, the mass of atomic Cs, and transition dipole moment corresponding to the $6\,^2S_{1/2}\rightarrow 6\,^2P_{3/2}$ atomic Cs transition. The initial internal ground state was taken to be $m_j=-1/2$ and the initial Gaussian distribution of the perpendicular motion was centered around $k_z^i=0.87$ nm^{-1} with a width parameter $\xi=5.00$ nm. The inital transverse momentum is taken to be $k_x^i=0.73$ nm^{-1}, $k_y^i=0.0$. This corresponds approximately to cold Cs atoms produced in a magneto-optic trap after a free fall of about 1.5 cm before colliding with the nanostructured surface inclined at an angle of about 40° between the vertical axis and the surface normal. Under these conditions, the incoming and specular direction are in the $y=0$ plane, as indicated in Fig. 1. We found converged results for a cutoff distance of about 600 nm. The asymptotic wave function is then analyzed to yield the diffraction probabilities $P(m,n)$ as outlined in the preceding section. As will be discussed in Sec. IV B, most of the diffraction is ''out of plane'' along the y axis. Therefore in all calculations, grids of only 16 points on the x axis were needed while computation along axes y and z required 64 and 1024 points, respectively, for convergence.

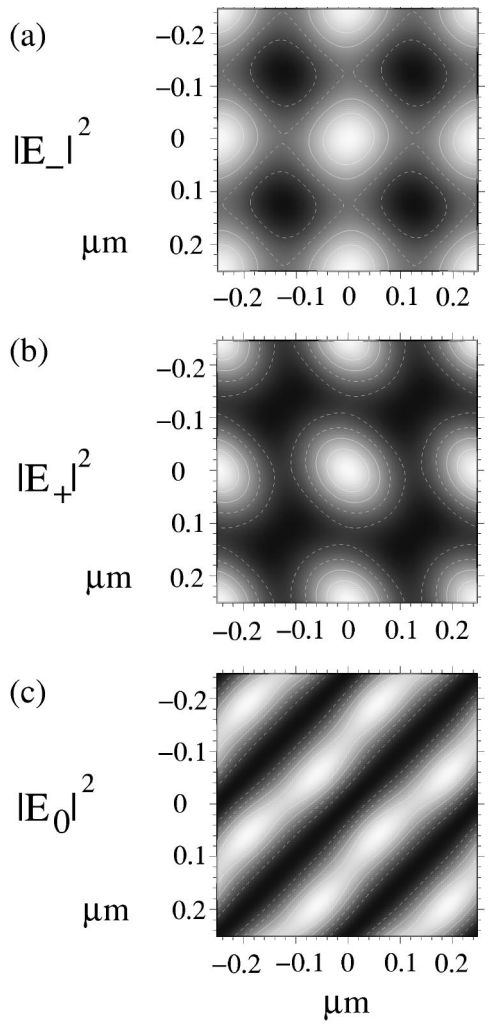

FIG. 5. Distribution of the spherical components of the electric field 125 nm above the top of the nanostructures. The contour lines correspond to (in units of $|E_i|^2$) (a) 0.377, 0.387 (dashed lines) and 0.397, 0.407 (solid lines), (b) 0.020, 0.025 (dashed lines) and 0.030, 0.035 (solid lines), (c) 2.3×10^{-4}, 4.6×10^{-4} (dashed lines) and 6.9×10^{-4}, 9.2×10^{-4} (solid lines).

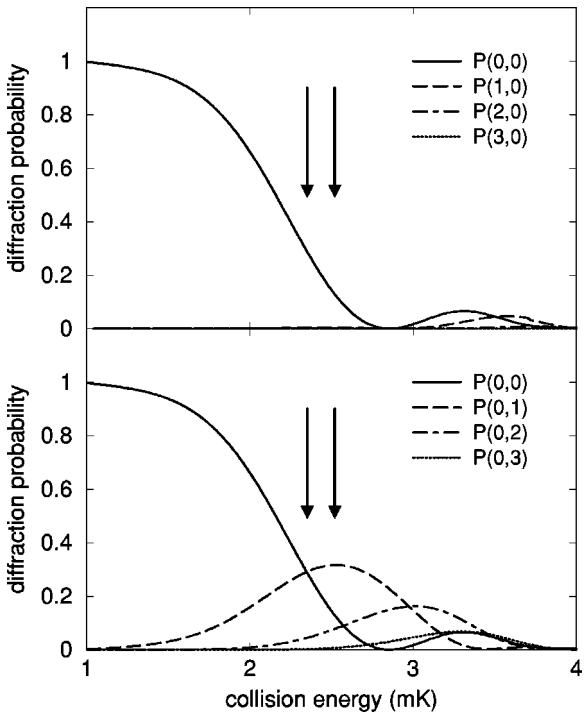

FIG. 6. Upper panel, in-plane diffraction probability $P(m,0)$ (the plane containing $\mathbf{k}_i$). Lower panel, out-of-plane diffraction probability $P(0,n)$ (perpendicular to the plane containing $\mathbf{k}_i$), as a function of total collision energy($\mathcal{E}=k_BT$). The arrows indicate the cases discussed in the text.

IV. RESULTS

A. Subwavelength optical near field

In Fig. 3 we show the geometry of the TiO_2 cubes (top) together with the intensity distribution (bottom) at a distance of 125 nm above the surface. The arrow indicating the plane of incidence of the laser beam is denoted by $\mathbf{k}_{00}^{\parallel}$ and plane of incidence of the atoms by $\mathbf{k}_i$. One can clearly see that the light fields bear the periodicity of the nanostructures. We found that illuminating the nanostructures with the plane of laser incidence aligned along the cube diagonals rather than along the sides yields periodic potentials with steeper gradients (more pronounced localization) even at distances far above the surface. At the illustrated distance of 125 nm above the surface, we still find pronounced periodic field intensity modulation. This strong localization of light intensity above high-refractive-index structures is a well-known characteristic of the TM illumination mode. It has been theoretically modeled and experimentally verified by the SNOM technique for a number of nanostructured objects [4]. In Fig. 4 we show a cross section of the field intensity distribution in the y,z plane above the nanostructures upto 400 nm. One clearly sees how the intensity contrast above the nanostructures decays with increasing distance. Depending on the kinetic energy, the falling atoms will penetrate to different heights above the surface, therefore experiencing a different amplitude modulation (contrast) at the plane of the mean classical turning point. It is important to note that even if the contrast diminishes with distance, the periodicity remains the same; and that even if the atoms are diffracted at large distances from the surface, the diffraction angle will still be controlled by the ratio of the atom de Broglie wavelength to the optical grating period. In order to rigorously establish the optical potential that governs the atomic motion, we need the full information of the field above the surface, i.e., the three spherical components of the electric field E_+, E_-, and E_0, as can be seen from Eq. (8). The quantization axis was chosen to be perpendicular to the plane of laser incidence. From Fig. 5 one can see that the different components of the light fields are a complicated function of space that will interact with the multilevel internal structure of the colliding atom. Note that the E_0 component is one order of magnitude smaller than E_+ or E_-.

B. Diffraction probabilities including ground-state degeneracy

In this section, we show the results for diffractive scattering, using the light-field parameters as detailed in the preced-

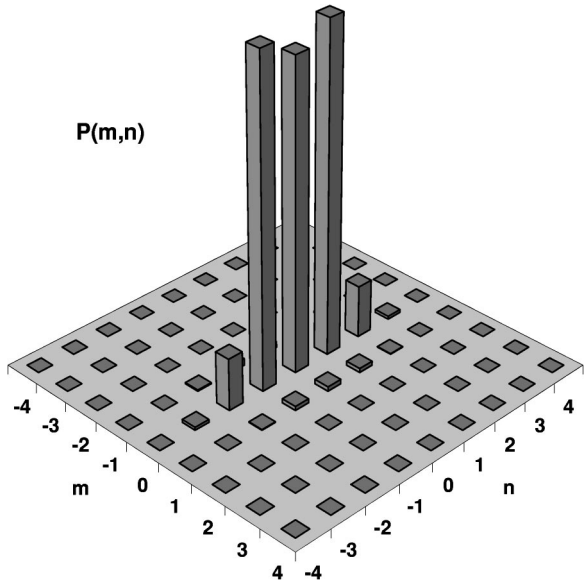

FIG. 7. Diffraction probabilities $P(m,n)$ for Cs atoms with a total energy of 2.35 mK corresponding to a drop height of 15 mm (left arrows in Fig. 3) and an angle of incidence (between the vertical axis and the surface normal) of 40°. The diffraction angle between the orders $(0,\pm 1)$ is $\simeq 2.6°$.

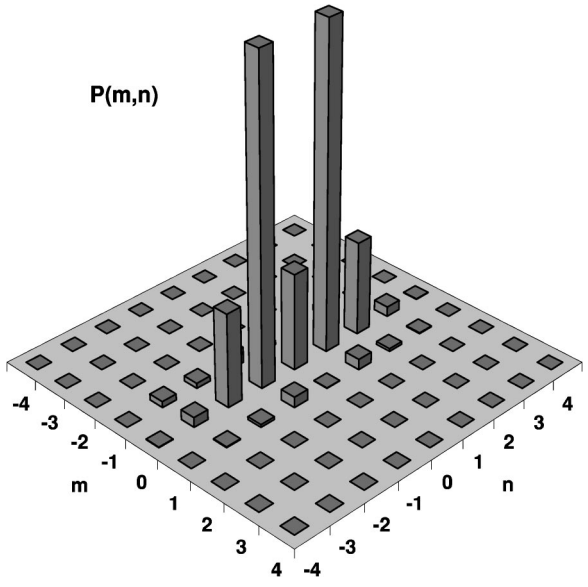

FIG. 8. Same as Fig. 7, but for a total energy of 2.56 mK, corresponding to a drop height of 16 mm (right arrows in Fig. 6) and an angle of incidence of 38°. The diffraction angle between the orders $(0,\pm 1)$ is $\simeq 2.0°$.

ing section. We stress that these probabilities are calculated using the Cs $6\,^2S_{1/2} \rightarrow 6\,^2P_{3/2}$ transition dipole and atomic mass, but that no other specific atomic parameters were used. This particle is still a model atom, however, since we have ignored the hyperfine structure in the ground and excited states. The center-of-mass motion is treated entirely quantum mechanically, and the polarization state of the electric field with its spatial variation rigorously included in the calculations. Since we are considering a two-dimensional potential surface, the diffraction takes place in two spatial directions labeled $\mathbf{G}_{mn}$, which are the reciprocal lattice vectors corresponding to the x and y directions, respectively. The probability $P(m,n)$ to diffract into a given order (m,n) as a function of energy is given by Eq. (12). Figure 6 plots these diffraction probabilities $P(m,0)$ (top panel) and $P(0,n)$ (bottom panel) as a function of total energy. The symmetrical results for negative values of m,n are not shown for clarity. With the definitions employed $(m,0)$ corresponds to diffraction within the plane of incidence of the atoms while $(0,n)$ corresponds to diffraction perpendicular to this plane. These two cases will be called ''in-plane'' and ''out-of-plane'' diffraction, respectively. Comparing the top and bottom panels of Fig. 6, we see that probabilities for in-plane and out-of-plane diffraction differ dramatically.

The top panel of Fig. 6 shows the in-plane diffraction probability as a function of energy for fixed initial transverse momentum of $k_i^x = 0.73\ \mathrm{nm}^{-1}$. For low energies, we find negligible diffraction. Most of the final population is in the (0,0) channel, which represents specular reflection. As the energy $\mathcal{E}$ increases, $P(0,0)$ decreases and falls off to almost zero for energies greater than 2.5 mK ($\mathcal{E} = k_B T$). The higher orders of in-plane diffraction $P(m,0)$, $m = \pm 1, \pm 2, \pm 3, \ldots$ are not significantly populated either. The bottom panel of Fig. 6 shows where the scattering flux has gone. Almost the entire population is found in the out-of-plane diffraction orders $(0,n)$, $n = \pm 1, \pm 2, \pm 3$. The fact that we calculate a rapidly decreasing in-plane diffraction corresponds to the well-known averaging of the transverse scattering amplitude of the atomic motion parallel to the diffracting structures [22]. With our parameters, we find an interaction time of about 3 μsec, which together with the initial transverse momentum of $k_i^x = 0.73\ \mathrm{nm}^{-1}$ implies that the atoms ''sample'' the modulated potential over a transverse distance of about 800 nm, greater than the periodicity of the potential by more than a factor of three. For the out-of-plane scattering there is no such averaging and the situation is analogous to in-plane diffraction at normal incidence. It is worth noting that this out-of-plane diffraction at grazing incidence (in a quite different experimental arrangement than the one envisaged here) has been observed experimentally [53].

Using the results shown in Fig. 6, one can now simply read off the probability for specific collision energies. At an energy of 2.35 mK, which corresponds to an angle of incidence of about 40° (indicated by the left arrows in the top and bottom panels of Fig. 6), we have almost the entire population equally distributed in the three diffraction orders (0,0) and $(\pm 1,0)$. Figure 7 shows the complete set of diffraction probabilities $P(m,n)$ for this case. One sees clearly that the only significant diffraction is out-of-plane, and the three dominating diffraction channels have almost equal probability of 30% each. The diffraction angle, given roughly by the ratio of de Broglie wavelength to grating periodicity, is quite large—about 2.6°. This geometry could thus be very attractive for the realization of an atomic beam splitter or for atomic interferometry.

As a second example, we have shown in Fig. 8 the situation at slightly higher collision energy of 2.52 mK. With the chosen initial transverse momentum this corresponds to an

angle of incidence of about 38°. The maximum of the final state population is now concentrated in the orders $(0,\pm 1)$ while the specular direction is suppressed to about 10%. At this slightly higher energy, we find also the diffraction peaks $(0,\pm 2)$ to be populated. Still, the ratio between $P(0,0)$ [or $P(0,\pm 2)$] and $P(0,\pm 1)$ is about 3, and the angle spanned by the two main diffraction peaks $P(0,1)$ and $P(0,-1)$ is about 2°.

C. Diffraction probabilities neglecting ground-state degeneracy

In the preceding section, we have calculated the diffraction probability including the ground-state degeneracy. As can be seen from Eq. (8), the intricate spatial distributions of polarization in general do not allow treatment of the problem as a one-surface scattering event, but require the solution of multiple internal states coupled to the optical potential. However, as one sees from Fig. 3, the electric field is dominated by the E_+ and E_- components, with the E_0 one order of magnitude smaller (the axis for the polarization state is chosen to be orthogonal to the plane of incidence of the laser beam). One sees from Eq. (8) that the coupling between the ground-state sublevels in the present case of an $S_{1/2}\rightarrow P_{3/2}$ transition is due to the E_0 component. Hence if the component E_0 is sufficiently small, the system of Eqs. (6) and (8) decouples and we have the situation of an effective single-surface collision. Consistent with this observation, we find that, starting from a well-defined initial m_j level, less than 0.1% of the population is transferred to the other one. As a consequence, one can assume that a treatment on one surface only, which greatly simplifies the computational burden, can yield satisfactory results. Thus in this particular case a one-surface calculation gives very good agreement with the full results, even for the weakly populated diffraction orders. In general, however, with atoms having higher ground-state multiplicity and with different optical materials and excitation geometries, a full coupled-surface calculation will be necessary.

V. CONCLUSIONS

In this paper we have investigated the diffraction of cold atoms by highly structured subwavelength optical potentials generated from evanescent fields. Our approach includes a three-dimensional quantum treatment of the atomic center of mass motion. We take into account the spatial distribution of rapidly varying polarization states of the nanostructured optical fields and include the effect of these polarization changes on the atom ground internal state populations.

As an illustration, we have chosen a model system that corresponds to cold cesium atoms (without nuclear spin) diffracting from a nanostructured surface illuminated under conditions of total internal reflection. The interaction of cold atoms with these light fields is calculated in the limit of large detuning and negligible absorption. For experimentally realistic initial conditions, we find diffraction angles of the order of 2° with about two third of the initial atomic flux concentrated in the first two diffraction orders. These structures may therefore prove useful in wide-angle atomic interferometers.

ACKNOWLEDGMENTS

Financial support from the Ministère d'Education Nationale, Recherche et Technologie, the Centre National de Recherche Scientifique, the program Action Coordonnée Optique, and the Région Midi-Pyrénées is gratefully acknowledged. Stimulating discussions with D. Lemoine are also gratefully acknowledged.

[1] A useful entry to the literature of atom optics and atom interferometry is *Atom Interferometry*, edited by P. R. Berman (Academic Press, New York, 1997).
[2] C.C. Bradley, W.R. Anderson, J.J. McClelland, and R.J. Celotta, Appl. Surf. Sci. **141**, 210 (1999).
[3] J.J. McClelland, in *Handbook of Nanostructured Materials and Nanotechnology*, edited by H.S. Nalwa (Academic Press, San Diego, CA, 2000), Vol. 1, pp. 335–385.
[4] C. Girard and A. Dereux, Rep. Prog. Phys. **59**, 657 (1996).
[5] C. Girard, C. Joachim, and S. Gauthier, Rep. Prog. Phys. **63**, 893 (2000).
[6] J.-J. Greffet and R. Carminati, Prog. Surf. Sci. **56**, 133 (1997).
[7] J.P. Dowling and J. Gea-Banacloche, Adv. At., Mol., Opt. Phys. **37**, 1 (1996).
[8] A.H. Barnett, S.P. Smith, M. Olshanni, K.S. Johnson, A.W. Adams, and M. Prentiss, Phys. Rev. A **61**, 023608 (2000).
[9] J.P. Burke, S.-T. Chu, G.W. Bryant, C.J. Williams, and P.S. Julienne (unpublished).
[10] J.D. Weinstein and K.G. Libbrecht, Phys. Rev. A **52**, 4004 (1995).
[11] D. Muller, E.A. Cornell, M. Prevedelli, P.D.D. Schwindt, A. Zozulyz, and D.Z. Anderson, Opt. Lett. **25**, 1382 (2000).
[12] D. Cassettari, B. Hessmo, R. Folman, T. Maier, and J. Schmiedmayer, Phys. Rev. Lett. **85**, 5483 (2000).
[13] W. Hänsel, J. Reichel, P. Hommelhoff, and T.W. Hänsch, Phys. Rev. Lett. **86**, 608 (2001).
[14] N.H. Dekker, C.S. Lee, V. Lorent, J.H. Thywissen, S.P. Smith, M. Drndic, R.M. Westervelt, and M. Prentiss, Phys. Rev. Lett. **84**, 1124 (2000).
[15] E.A. Hinds, *Atomic Physics*, edited by E. Arimondo, P. de Natale, and M. Inguscio (American Institute of Physics, New York, 2001), Vol. 17, p. 405.
[16] E.A. Hinds, C.J. Vale, and M.G. Boshier, Phys. Rev. Lett. **86**, 1462 (2001).
[17] W. Hänsel, P. Hommelhoff, T.W. Hänsch, and J. Reichel, Nature (London) **413**, 498 (2001).
[18] H. Ott, J. Fortagh, G. Schlotterbeck, A. Grossmann, and C. Zimmermann, Phys. Rev. Lett. **87**, 230401 (2001).
[19] P.L. Gould, G.A. Ruff, and D.E. Pritchard, Phys. Rev. Lett. **56**, 827 (1986), and references cited therein.
[20] R.J. Cook and R.K. Hill, Opt. Commun. **43**, 258 (1982).
[21] For early work see C. Adams, M. Siegel, and J. Mlynek, Phys.

Rep. **240**, 143 (1994), and references cited therein.
[22] C. Henkel, H. Wallis, N. Westbrook, C.I. Westbrook, A. Aspect, K. Sengstock, and W. Ertmer, Appl. Phys. B. Laser Optics **B69**, 277 (1997).
[23] K. Kobayashi, S. Sangu, H. Ito, and M. Ohtsu, Phys. Rev. A **63**, 13806 (2000).
[24] V.I. Balykin, D.A. Lapshin, M.V. Subbotin, and V.S. Letokhov, Opt. Commun. **145**, 322 (1998).
[25] C. Henkel, K.M. Olmer, R. Kaiser, and C.I. Westbrook, Phys. Rev. A **56**, R9 (1997).
[26] R. Marani, L. Cognet, V. Savalli, N. Westbrook, C.I. Westbrook, and A. Aspect, Phys. Rev. A **61**, 53402 (2000).
[27] G. Lévêque, C. Girard, G. Colas des Francs, J.C. Weeber, C. Meier, C. Robillard, R. Mathevet, and J. Weiner, Phys. Rev. E **65**, 036701 (2002), and e-print physics/0111177.
[28] B. Jackson, Annu. Rev. Phys. Chem. **46**, 251 (1995).
[29] *Time Dependent Quantum Mechanics*, Vol. 299 of *NATO Advanced Study Institute, Series B: Physics*, edited by J. Broeckhove and L. Lathouwers (1992).
[30] C. Meier and U. Manthe, J. Chem. Phys. **115**, 5477 (2001).
[31] G.-J. Kroes, Prog. Surf. Sci. **60**, 1 (1999).
[32] D. Lemoine, J. Chem. Phys. **101**, 4343 (1994).
[33] G.C. Corey and D. Lemoine, J. Chem. Phys. **97**, 4115 (1992).
[34] M.-N. Carre, B. Jackson, and D. Lemoine, J. Chem. Soc., Faraday Trans. **93**, 949 (1997).
[35] G.-J. Kroes, J.G. Snijders, and R.C. Mowrey, J. Chem. Phys. **102**, 5512 (1995).
[36] M.-C. Heitz and H.-D. Meyer, J. Chem. Phys. **114**, 1382 (2001).
[37] M. Ehara, H.-D. Meyer, and L.S. Cederbaum, J. Chem. Phys. **105**, 8865 (1996).
[38] R. Millot and A.P.J. Jansen, J. Chem. Phys. **109**, 1966 (1998).
[39] J.L. Kann, T.D. Milster, F.F. Froehlich, R.W. Ziolkowski, and J.B. Judskins, J. Opt. Soc. Am. A **12**, 1677 (1995).
[40] R. Petit, *Electromagnetic Theory of Gratings* (Springer Verlag, Heidelberg, 1980), Vol. 22.
[41] D. Maystre and M. Nevière, J. Opt. **9**, 301 (1978).
[42] F. Montiel and M. Nevière, J. Opt. Soc. Am. A **11**, 3241 (1994).
[43] C. Girard, A. Dereux, and O.J.F. Martin, Phys. Rev. B **49**, 13 872 (1994).
[44] O.J.F. Martin, C. Girard, D.R. Smith, and S. Schultz, Phys. Rev. Lett. **82**, 315 (1999).
[45] C.M. Savage, D. Gordon, and T.C. Ralph, Phys. Rev. A **52**, 4741 (1995).
[46] R.C. Mowrey and D.J. Kouri, J. Chem. Phys. **84**, 6466 (1986).
[47] D. Feit, J.A. Fleck, and A. Steiger, J. Comput. Phys. **47**, 412 (1982), J.A. Fleck, J.R. Morris, and M.D. Feit, Appl. Phys. **10**, 129 (1976).
[48] D. Kosloff and R. Kosloff, J. Comput. Phys. **52**, 35 (1983).
[49] M.H. Beck, A. Jäckle, G.A. Worth, and H.-D. Meyer, Phys. Rep. **324**, 1 (2000).
[50] D. Lemoine, J. Chem. Phys. **101**, 4350 (1994).
[51] G.-J. Kroes, M.R. Wall, J.P. Pang, and D. Neuhauser, J. Chem. Phys. **106**, 1800 (1997).
[52] A. Landragin, J.-Y. Courtois, G. Labeyrie, N. Vansteenkiste, C.I. Westbrook, and A. Aspect, Phys. Rev. Lett. **77**, 1464 (1996).
[53] R. Brouri, R. Asimov, M. Gorlicki, S. Feron, J. Reinhardt, V. Lorent, and H. Haberland, Opt. Commun. **124**, 448 (1996).